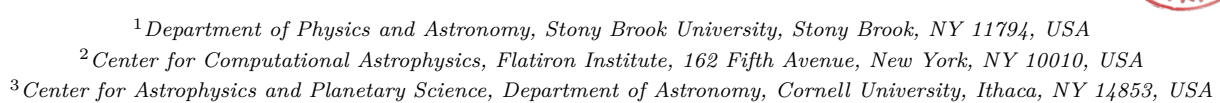
Global simulation of thermal torques

Sabina Sagynbayeva, 1,2 Rixin Li (李目新),3 and Philip J. Armitage 1,2



ABSTRACT

1. INTRODUCTION

Circumplanetary disks (CPDs) are believed to be a natural byproduct of the planet formation process, arising from the vertical infall of gas from the protoplanetary disk onto the growing protoplanet (Ward & Canup 2010). Simulations have shown that CPDs exhibit complex dynamics affected by viscosity, thermal structure, magnetic fields, and turbulence (Fujii et al. 2011; Gressel et al. 2013; Szulágyi et al. 2014). Early numerical studies utilized two-dimensional hydrodynamic models to demonstrate disk formation and characterize basic properties like size and density distribution (D'Angelo et al. 2003). Later work incorporated three-dimensional simulations to better capture non-axisymmetric flows and vertical disk structure (Machida et al. 2008).

A major limitation of early models was the use of simplified thermodynamic treatments like locally isothermal equations of state. Recent research has focused on more realistic energy equations to determine the effects of radiation transport, viscous heating, and radiative cooling on CPD structure and evolution (Szulágyi et al. 2016; Zhu & Baruteau 2016). Thermal physics can alter turbulence and angular momentum transport in the disk, which may affect accretion onto the planet. Other areas of active research include studying magnetic field amplification through MRI-driven turbulence (Fujii et al. 2014), exploring disk chemistry and composition (Fujii et al. 2017), and analyzing impacts of planet mass and orbital properties (Szulágyi et al. 2017).

CPDs have also long been hypothesized to be the birthplaces of regular moons around giant planets (Lunine & Stevenson 1982; Canup & Ward 2006). However, the efficiency of satellite formation within CPDs depends on several factors that remain poorly constrained. Early analytic work suggested disks may be too compact

and short-lived to readily form large moons (Goodman & Rafikov 2001). But recent hydrodynamic simulations indicate CPDs can exhibit extended disks over 100s of planetary radii and lifetimes over 1000 orbits (Szulágyi et al. 2016; Fujii et al. 2017).

Higher resolution 3D MHD models reveal turbulence and instabilities that could concentrate solids and aid satellite growth. Analysis of pebble accretion shows Galilean moon formation may be possible in CPDs around Jupiter-like planets (Shibaike et al. 2017; Ronnet et al. 2018).

2. METHODS

2.1. Disk model

Isentropic disk model from Fung et al. (2017). The simulations are performed in spherical coordinates, where r, ϕ , and θ denote the usual radial, azimuthal, and polar coordinates, respectively.

$$\Phi = -\frac{G(M_* + M_p)}{1 + q} \left[\frac{1}{r} + \frac{q}{\sqrt{r^2 + R_p^2 - 2rR_p \cos \phi' + \epsilon^2}} - \frac{qR \cos \phi'}{R_p^2} \right]$$
(1)

In eq. 1, $q = M_p/M_*$ is the mass ratio of a protoplanet to a star, ϵ is the smoothing length of the planet's potential, and $\phi' = \phi - \phi_p$ denotes the azimuthal separation from the planet. GM = 1, $R_p = 1$.

Keplerian velocity $v_k = \sqrt{\frac{GM}{r}}$ and keplerian frequency $\Omega_k = \sqrt{\frac{GM}{r^3}}$ equal to 1 at the planet's orbit. v_p - planet's orbital speed. $q=1.5\times 10^{-5}\approx 5M_\oplus$

The planet is introduced to the disk gradually, where its mass increases to the desired value over the first orbit.

The simulation domain spans $0.65R_p$ to $1.35R_p$ in the radial, and the full 2π in azimuth.

The Hill radius of a planet is:

$$r_H = R_p \left(\frac{q}{3}\right)^{\frac{1}{3}} \tag{2}$$

 r_s is a small fraction of r_H , between 3% to 10% of r_H . The isentropic equation of state:

$$p = \frac{c_0^2 \rho_0}{\gamma} \left(\frac{\rho}{\rho_0}\right)^{\gamma} \tag{3}$$

In Eq. 3, c_0 is the isothermal sound speed when $\rho = \rho_0 = 1$. The disk's scale height H = 0.05 scales the sound speed as $c_0 = H\Omega = 0.05$.

2.1.1. Initial conditions

For hydrostatic equilibrium:

$$\rho = \rho_0 \left[\left(\frac{R}{R_p} \right)^{\left(-\beta + \frac{3}{2}\right) \frac{2(\gamma - 1)}{\gamma + 1}} - \frac{GM(\gamma - 1)}{c_0^2} \left(\frac{1}{R} - \frac{1}{r} \right) \right]^{\frac{1}{\gamma - 1}}$$

$$(4)$$

 $\beta = \frac{3}{2}$ defines the surface density profile $\Sigma \propto R^{-\beta}$. The orbital frequency of the disk:

$$\Omega = \sqrt{\Omega_k^2 + \frac{1}{r\rho} \frac{\partial P}{\partial r}} \tag{5}$$

REFERENCES

Canup, R. M., & Ward, W. R. 2006, Nature, 441, 834, doi: 10.1038/nature04860

D'Angelo, G., Henning, T., & Kley, W. 2003, ApJ, 599, 548, doi: 10.1086/379224

Fujii, Y. I., Kobayashi, H., Takahashi, S. Z., & Gressel, O. 2017, AJ, 153, 194, doi: 10.3847/1538-3881/aa647d

Fujii, Y. I., Okuzumi, S., & Inutsuka, S.-i. 2011, ApJ, 743, 53, doi: 10.1088/0004-637X/743/1/53

Fujii, Y. I., Okuzumi, S., Tanigawa, T., & Inutsuka, S.-i. 2014, ApJ, 785, 101, doi: 10.1088/0004-637X/785/2/101

Fung, J., Masset, F., Lega, E., & Velasco, D. 2017, The Astronomical Journal, 153, 124, doi: 10.3847/1538-3881/153/3/124

Goodman, J., & Rafikov, R. R. 2001, ApJ, 552, 793, doi: 10.1086/320572

Gressel, O., Nelson, R. P., Turner, N. J., & Ziegler, U. 2013, ApJ, 779, 59, doi: 10.1088/0004-637X/779/1/59

Lunine, J. I., & Stevenson, D. J. 1982, Icarus, 52, 14, doi: 10.1016/0019-1035(82)90166-X

$$v_r = v_\theta = 0$$

2.1.2. Grid setup

We use spherical-polar grid with a nested static mesh refinement (SMR) around the location of the planet. The intervals that span in radial, polar, and azimuthal directions are [0.4, 2.5], $[9\pi/20, 11\pi/20]$, and $[0, 2\pi]$, respectively. Aiming for 50 cells around the Hill's sphere, we came up with the effective resolution at the root level: 168 cells across the r-direction, 576 cells across the ϕ -direction, and 72 cells across the θ -direction.

Nested SMR that we implemented helped us to lower the resolution at the root level keeping high enough resolution around the Hill's sphere to resolve the CPD properly. The detailed description of the finest of the refined regions is shown on Table 2.1.2. The definitions of the normalization units and the corresponding values are listed in Table 2.1.2.

2.1.3. Resolution

2.2. Athena++ simulations

3. RESULTS

4. DISCUSSION

Refinement #1	$9\pi/20 \rightarrow 11\pi/20$	θ
	$0.8 \rightarrow 1.2$	r
	± 0.2	ϕ
Refinement #2	$19\pi/40 \rightarrow 21\pi/40$	θ
	$0.9 \rightarrow 1.1$	r
	± 0.1	ϕ
Refinement #3	$39\pi/80 \rightarrow 41\pi/80$	θ
	$0.95 \rightarrow 1.05$	r
	± 0.05	ϕ

Machida, M. N., Kokubo, E., Inutsuka, S.-i., & Matsumoto, T. 2008, ApJ, 685, 1220, doi: 10.1086/590421

Ronnet, T., Mousis, O., Vernazza, P., Lunine, J. I., & Crida, A. 2018, AJ, 155, 224,

doi: 10.3847/1538-3881/aabcc7

Shibaike, Y., Okuzumi, S., Sasaki, T., & Ida, S. 2017, ApJ, 846, 81, doi: 10.3847/1538-4357/aa8454

Szulágyi, J., Masset, F., Lega, E., et al. 2016, MNRAS, 460, 2853, doi: 10.1093/mnras/stw1160

Table 1. Normalization Units and Corresponding Values

Quantity	Unit
Length	r_p
Velocity	v_{K0}
Time	r_p/v_{K0}
Density	$ ho_0$
Pressure	$\rho_0 v_{K0}^2$
Mass accretion rate	$\rho_0 r_p^2 v_{K0}$

Szulágyi, J., Mayer, L., & Quinn, T. 2017, MNRAS, 464, 3158, doi: 10.1093/mnras/stw2617

Szulágyi, J., Morbidelli, A., Crida, A., & Masset, F. 2014, ApJ, 782, 65, doi: 10.1088/0004-637X/782/2/65

Ward, W. R., & Canup, R. M. 2010, AJ, 140, 1168, doi: 10.1088/0004-6256/140/5/1168

Zhu, Z., & Baruteau, C. 2016, MNRAS, 458, 3918, doi: 10.1093/mnras/stw202